Combined physical and pharmacological anabolic osteoporosis therapies synergistically increase bone response and local mechanoregulation

Authors: Friederike A. Schulte[1], Francisco C. Marques[1], Julia K. Griesbach[1], Claudia Weigt[1], Marcella von Salis-Soglio[1], Floor M. Lambers[1], Clemens Kreutz[2], Michaela Kneissel[2], Peter J. Richards[2,3], Gisela A. Kuhn[1], Ralph Müller[1]*

[1]Institute for Biomechanics, ETH Zurich; Zurich, Switzerland.

[2]Musculoskeletal Disease Area, Novartis Institutes for Biomedical Research; Basel, Switzerland.

[3]Bone and Stem Cell Research Group, CABMM, University of Zurich; Zurich, Switzerland.

*Corresponding author. Email: ram@ethz.ch

Abstract: Bone's ability to adapt to mechanical demands is governed by mechanoregulation, the process by which cells sense and respond to mechanical stimuli to maintain skeletal integrity. In osteoporosis, increased bone resorption activity leads to structural deterioration and elevated fracture risk. While existing pharmacological therapies aim to restore bone mass to reduce fracture risk, it is unclear how they modulate mechanoregulation, especially when combined with physical interventions. Here, we investigate the joint effects of load-bearing physical and pharmacological treatment in a female mouse model of osteoporosis using longitudinal *in vivo* micro-computed tomography and computational mechanics. We demonstrate that mechanical loading additively and synergistically enhanced predicted strength, bone volume, and mechanoregulation parameters when combined with anabolic therapies (parathyroid hormone and sclerostin antibody) but not with anti-catabolic treatments (bisphosphonates). Increases in predicted strength were associated with reductions in bone resorption rates, shifts in the (re)modeling thresholds as anticipated by Frost in the mechanostat theory, and the modeling capacity of anabolic pharmacological treatments. These findings underscore the therapeutic potential of combining anabolic pharmacological therapies with load-bearing physical activity, particularly in early treatment phases, to optimize bone adaptation and fracture prevention in osteoporosis management.

Introduction

Postmenopausal osteoporosis in women is characterized by increased bone resorption, leading to structural deterioration of the bone micro-architecture and increased susceptibility to fractures[1]. Exercise is fundamental to bone health, but its role alongside pharmacological treatment remains an area of active inquiry[2]. Patients with diagnosed osteoporosis often question the compatibility of exercise with pharmacological treatment, some fearing interference with drug efficacy, others assuming that their potent medications obviate the need for physical activity. This highlights the need for evidence on whether mechanical loading improves outcomes for bone strength beyond pharmacological monotherapy.

Mechanical loads are transmitted from the organ to bone cells, where osteocytes act as mechanosensors, osteoblasts form, and osteoclasts resorb bone. This interplay drives both remodeling (formation followed by resorption) and modeling (formation without prior resorption), the latter potentially via lining cell redifferentiation in the absence of sclerostin[3]. Key signaling pathways between bone cells include Wnt/beta-catenin[4] (osteocyte-osteoblast) and RANKL/OPG[5] (osteoblast-osteoclast). To study these dynamic processes *in vivo*, high-resolution imaging techniques such as micro-computed tomography (micro-CT) are commonly used. While micro-CT does not resolve individual cells or molecular signals, it captures the net microstructural changes resulting from formation and resorption, which are collectively referred to as bone (re)modeling[6].

On the cellular level, anti-resorptive bisphosphonates (BIS) prevent osteoclast attachment and activity by binding to hydroxyapatite crystals in the bone matrix, and are characterized by low osteoanabolic capacity[7]. We hypothesized that mechanical loading would stimulate bone formation, but bisphosphonates might blunt this response by inhibiting (re)modeling.

Intermittent parathyroid hormone (PTH) exerts anabolic effects by binding to PTH-receptors on osteoblasts and osteocytes, leading to suppression of sclerostin expression and subsequent activation of the Wnt/β-catenin signaling pathway. This promotes osteoblastic activity and indirectly enhances osteoclast recruitment via upregulation of RANKL expression by osteoblasts[8]. PTH and mechanical loading have shown synergistic effects in cortical bone[9,10]. We hypothesized that in trabecular bone, their combination would suppress otherwise increased resorption, and concurrently stimulate bone formation[11].

Sclerostin antibodies (SclAB) inhibit a Wnt/β-catenin-signaling antagonist protein, promoting osteoblast activity and suppressing osteoclast activity[12]. Wnt/β-catenin-signaling is initiated when a Wnt ligand binds to a Frizzled family receptor and its co-receptor LRP5/6 on the surface of a cell, resulting in β-catenin stabilization and target gene transcription inside the cell[11]. We hypothesized mechanical loading in combination with SclAB would increase formation and decrease resorption further. Synergy may arise because mechanical loading downregulates sclerostin expression in osteocytes[13], while SclAB pharmacologically neutralizes it, amplifying the same pathway from two directions, especially in trabecular bone which particularly adapts its microarchitecture to mechanical demands. It should be noted that, similar to mechanical loading, sclerostin antibody effects saturate after a certain time, which limits their long-term use as a standalone therapy[14].

Frost's mechanostat theory[15-17] proposes that bone adapts to maintain mechanical strain within a defined setpoint range - much like a thermostat. The setpoints separate the four following states: the disuse state for bone resorption; the adapted state for quiescence, the overload state for formation, and the fracture state for microdamage and fractures. The mechanostat theory was introduced more than 30 years ago. In this theoretical construct, anti-catabolic bisphosphonates help inhibit increased bone resorption in underloaded areas by raising the mechanical setpoints towards higher strains. Anabolic treatments theoretically promote bone

formation by lowering the mechanical setpoints required to initiate formation, provided mechanical loading is also encouraged. Measuring the "setpoints" of osteoporosis medications in the context of Frost's mechanostat theory, however, is not straightforward, as the setpoints themselves are theoretical constructs that describe the mechanical thresholds at which bones adjust their structure, and measuring them experimentally would require complex assessments of both bone volume and mechanical strain under highly controlled conditions.

Here we provide experimental insights into this interaction using *in vivo* micro-computed tomography (micro-CT) and finite-element modeling in a C57BL/6 mouse model of osteoporosis. The aim of this study was to explore whether combining pharmacological treatments with mechanical loading leads to improved pharmacological treatment outcomes, i.e. stronger bones. We tested short-term effects of BIS, PTH, and SclAB treatment with or without mechanical loading of the 6th caudal vertebra, aiming to maximize bone accrual in early treatment phases. The choice of selected therapies was based on clinical relevance and distinct modes of action in the bone (re)modeling process.

Results

Micro-architectural and (re)modeling differences reveal treatment-specific effects on bone recovery after ovariectomy

As shown in Fig. 1a, C57BL/6 mice were ovariectomized at 15 weeks-of-age, and bone loss was confirmed in all animals (n=105) via *in vivo* micro-CT of the 6th caudal vertebra (-26.8 ± 0.95% change in bone volume fraction (BV/TV) from baseline). From week 20 to 24, animals received pharmacological and/or mechanical treatment through an established tail vertebra loading model[18].

111 In the VEH-group, BV/TV continued to decline, while all monotreatment groups showed
112 significant increases ($p<0.001$, Fig. 1b). Trabecular thickness (Tb.Th) did not increase
113 significantly in BIS compared to VEH, whereas all anabolic treatments led to increases, but
114 lower in PTH than in ML and SclAB ($p<0.01$, Fig. 1c). Trabecular number (Tb.N) was
115 preserved in BIS but was significantly lower in all other groups compared to BIS ($p<0.001$, Fig.
116 1d). Connectivity density (Conn.D) was preserved in BIS and PTH and declined in VEH, ML,
117 and SclAB ($p<0.05$, Fig. 1e). A full summary of these microstructural parameters is provided
118 in Supplementary Table S.2. As previously described[18], mechanical loading increases BV/TV
119 mainly through trabecular thickening despite a reduction in trabecular number, explainable by
120 a full loss of thin trabeculae - a pattern also seen in the SclAB-group (Fig. 1c,d). In contrast,
121 PTH increased BV/TV through moderate thickening and sustained preservation of trabecular
122 number, resulting in a smaller loss of connectivity. BIS maintained BV/TV by preserving
123 existing trabeculae, including thinner ones, with minimal thickening (Fig. 1, b-e).

124 The micro-architectural changes resulted from the time course of formation and resorption (Fig.
125 1f). In week interval w20-22 (see also Supplementary Table S.5 for results from the second
126 interval, w22–24), bone formation rate per bone volume (BFR) was significantly increased in
127 ML and PTH compared to VEH, with no significant increases in BIS or SclAB (Fig. 1g).
128 Mineral apposition rate (MAR) did not differ between groups (Fig. 1h), while mineralizing
129 surface per bone surface (MS) was elevated in all treatment groups compared to VEH ($p<0.05$,
130 Fig. 1i). Bone resorption rate per bone volume (BRR) was significantly reduced in all treatment
131 groups versus VEH (Fig. 1j), where BRR in PTH was the least reduced (significantly higher
132 than VEH, ML, and BIS), consistent with the known anabolic effects of intermittent PTH
133 treatment. Surprisingly, BRR was found to be significantly lower than VEH, while not as low
134 as in ML and BIS. This decrease, even more pronounced in the second time interval (see
135 Supplementary material Table S.5), may result from micro-CT missing parts of the reversal

phase between resorption and formation, thus potentially underrepresenting remodeling at the same sites. As expected, mineral resorption rate (MRR) was significantly lower in the BIS-group compared to VEH and unchanged in the anabolic groups (Fig. 1k), suggesting bisphosphonates preserve Tb.N (Fig. 1d) by preventing full trabecular resorption. Eroded surface per bone surface (ES), reflecting the proportion of bone surface previously affected by resorption, was significantly lower in ML and SclAB compared to VEH, BIS, and PTH ($p<0.05$, Fig. 1l).

Together, these results confirm that each monotherapy exerted effects consistent with its known mode of action - bisphosphonates preserving trabecular structure by suppressing bone resorption, and anabolic agents increasing bone mass predominantly through formation - while also highlighting treatment-specific differences in trabecular architecture and dynamic turnover.

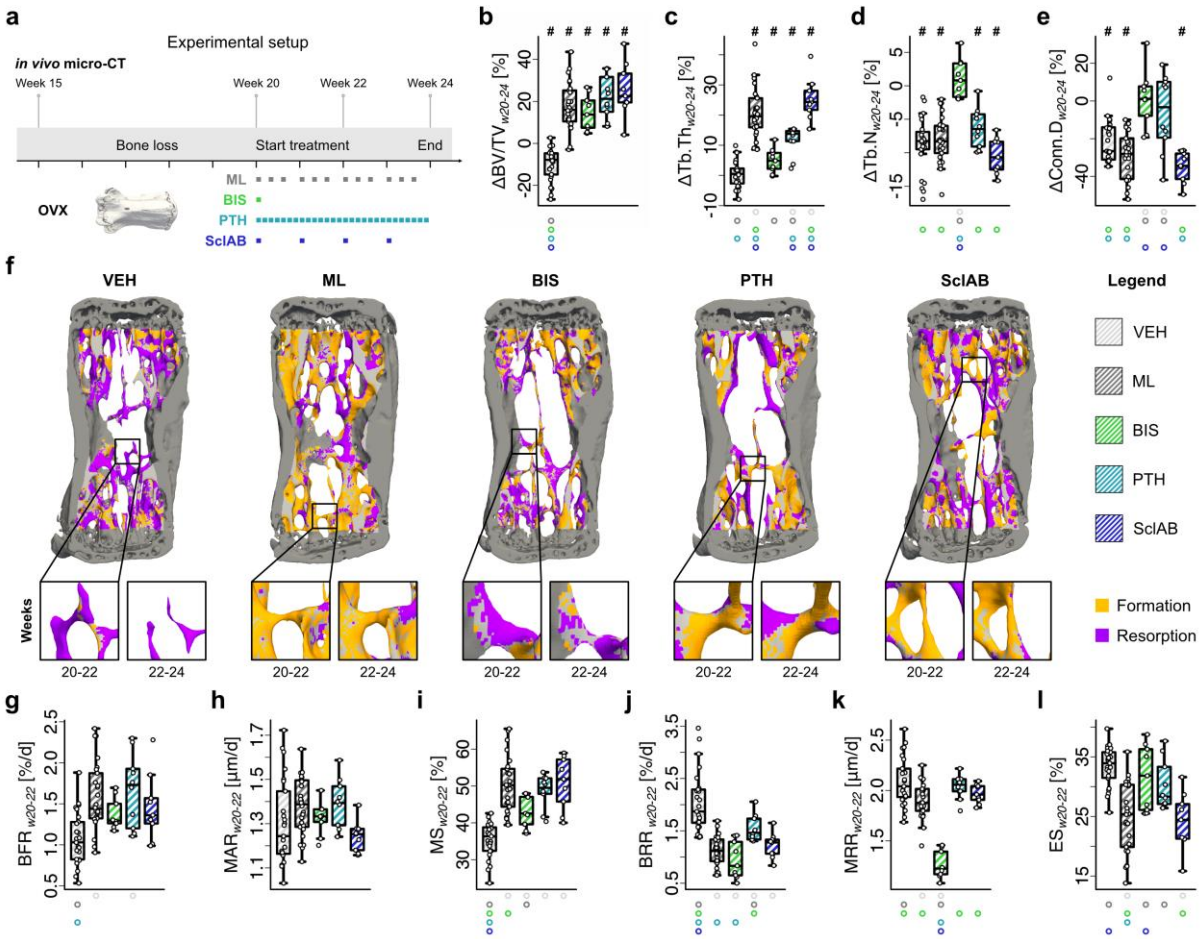

Figure 1: Osteoporosis monotreatments enhance trabecular bone micro-architecture by different mechanisms of action. *(**a**) Experimental setup. 15-week-old mice are ovariectomized and treatment is administered between week 20 (w20) and 24 (w24). (**b-e**) Monotreatments (VEH: n=29, BIS: n=9, PTH: n=10, SclAB: n=9), boxplots show percentage change in four weeks. in (**b**) bone volume fraction ΔBV/TV, (**c**) trabecular thickness ΔTb.Th, (**d**) trabecular number ΔTb.N (**e**) connectivity density ΔConn.D. The box spans the interquartile range (IQR) from the 25th to the 75th percentile. The median is shown as a line inside the box. Whiskers extend to the most extreme data points within 1.5 × IQR, points beyond this range are plotted as outliers. # indicates that the delta of the group is different from zero, as tested with t-test with null-hypothesis. (**f**) Representative micro-computed tomography overlays at intervals w20-w22 and w22-w24, with formation and resorption volumes (**g-l**) (Re)modeling rates calculated from time interval w20-w22 (**g**) bone formation rate per bone volume BFR (**h**) mineral apposition rate MAR (**i**) mineralizing surface per bone surface MS (**j**) bone resorption rate per bone volume BRR (**k**) mineral resorption rate MRR (**l**) eroded surface per bone surface ES. Significant differences are depicted with a symbol in the color of the corresponding group (o: to monotreatment, ●: to combined treatment, see Supplementary Table S.1 for color encoding, p<0.05).*

164 **Mechanical loading modulates structural and functional responses to pharmacological**
165 **interventions**

166 We next assessed how additional mechanical loading influenced the response to
167 pharmacological treatment. In the BIS + ML-group, BV/TV gains were significantly less than
168 the expected additive effects (treatment:loading: $p<0.05$, Fig. 2a), and did not differ
169 significantly from BIS alone (Supplementary Table S.2). In contrast, anabolic treatment
170 combined with mechanical loading (PTH + ML, SclAB + ML) resulted in additive increases,
171 as supported by a non-significant treatment:loading interaction (Fig. 2a). ΔTb.Th was
172 significantly higher in all combination groups compared to monotreatments after four weeks
173 (Fig. 2b). ΔTb.N was preserved in BIS + ML, despite the known Tb.N loss with ML alone (Fig.
174 2c), suggesting BIS blunted this effect. The loss of Tb.N observed in SclAB was not rescued in
175 SclAB + ML (Fig. 2c). Conn.D as a measure of the structural integrity and interconnectedness
176 of the trabecular network, was preserved the most in BIS + ML, and PTH + ML (Fig. 2d). It
177 should be noted that structural parameters such as Tb.Th and Tb.N are interdependent; apparent
178 increases in Tb.Th may arise from the loss of complete thinner trabeculae. Synergy was found
179 in total area (Tt.Ar), leading to additive increases in cortical area fraction (Ct.Ar/Tt.Ar) and
180 cortical thickness (Ct.Th), found in Supplementary Fig. S.1 and Table S.4. Predicted strength
181 increased in all treatment groups, with loading-induced increases being additive in the PTH +
182 ML group and synergistic in the SclAB + ML group ($p<0.05$, Fig. 2e). Strain energy density
183 (SED) decreased in all treatment groups, being most pronounced in the combination groups,
184 with less than the expected additive reduction in BIS + ML (treatment:loading: $p<0.05$, Fig. 2f,
185 Table 1). Illustrating the effect of decreasing SED, the visualization of the 6th caudal vertebra
186 in a SclAB + ML animal shows a highly loaded trabecula at week 20, followed by structural
187 reorganization and reduced SED at week 24 (see Fig. 2g). Linear regression analysis revealed

that the changes in predicted strength did not correlate with baseline BV/TV (R = 0.010) and moderately with Tb.Th (R = 0.424, Fig. 2h).

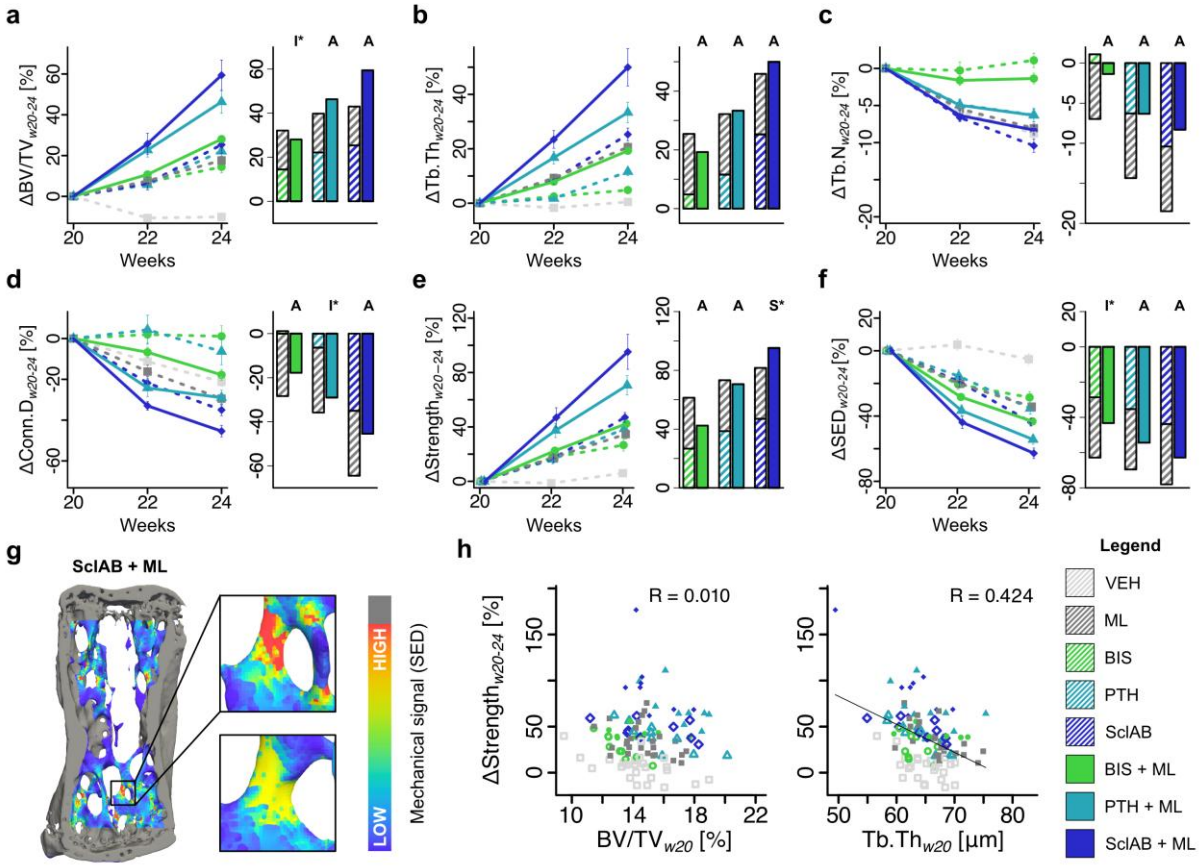

Figure 2: Mechanical loading increases the morphological effects of anabolic and anti-catabolic treatments, contributing to increased predicted strength. *(**a-f**) Changes from baseline in bone volume fraction (ΔBV/TV) (**b**) trabecular thickness (ΔTb.Th) (**c**) trabecular number (ΔTb.N) (**d**) connectivity density (ΔConn.D) (**e**) predicted strength (ΔStrength), and (**f**) strain energy density (ΔSED). Bars show group means of sum of single vs. combined treatment indicating: antagonistic (I), additive (A) or synergistic (S) effects determined via treatment:loading interaction in a linear model on the %-change. (**g**) Example of SED distribution in the 6th caudal vertebra of a ScIAB + ML animal, showing reduced SED after structural reorganization from week 20 to 24. (**h**) Linear regression of ΔStrength with BV/TV and Tb.Th at week 20.*

Combination treatments affect bone formation and resorption dynamics differentially

Bone formation rate per bone volume (BFR) was lowest in VEH and highest in the anabolic combination groups ($p<0.05$, Fig. 3a). MAR showed synergy in ScIAB + ML (treatment:loading: $p<0.05$, Fig. 3b). MS increased additively in PTH + ML and ScIAB + ML,

203 and antagonistically in BIS + ML (treatment:loading: $p<0.01$, Fig. 3c). Bone resorption rate per
204 bone volume (BRR) was reduced in all treatment groups ($p<0.05$, Fig. 3d). In BIS + ML, the
205 BRR reduction was antagonistically affected by mechanical loading (treatment:loading,
206 $p<0.05$). In contrast, BRR decreased synergistically in PTH+ML (treatment:loading: $p<0.05$,
207 Fig. 3d) and additively in SclAB + ML (Fig. 3d). MRR remained suppressed in BIS + ML and
208 was unaffected by mechanical loading (Fig. 3e). ES decreased synergistically in PTH + ML
209 treatment:loading: $p<0.05$, Fig. 3f) and SclAB + ML (treatment:loading: $p<0.01$, Fig. 3f). This
210 synergistic effect was, at least in SclAB + ML, still present in the second time interval (see
211 Supplementary Fig. S.2 and Table S.5 for results from w22–24). Representative trabecular
212 microstructures and insets of the combination groups at both time intervals are depicted in Fig.
213 3g. Changes in predicted strength correlated linearly with BFR ($R = 0.830$) and decayed
214 according to a power-law relationship with BRR ($\rho = 0.760$), indicating that small reductions
215 in bone resorption rates under treatment can result in large increases in predicted strength (Fig.
216 3h).

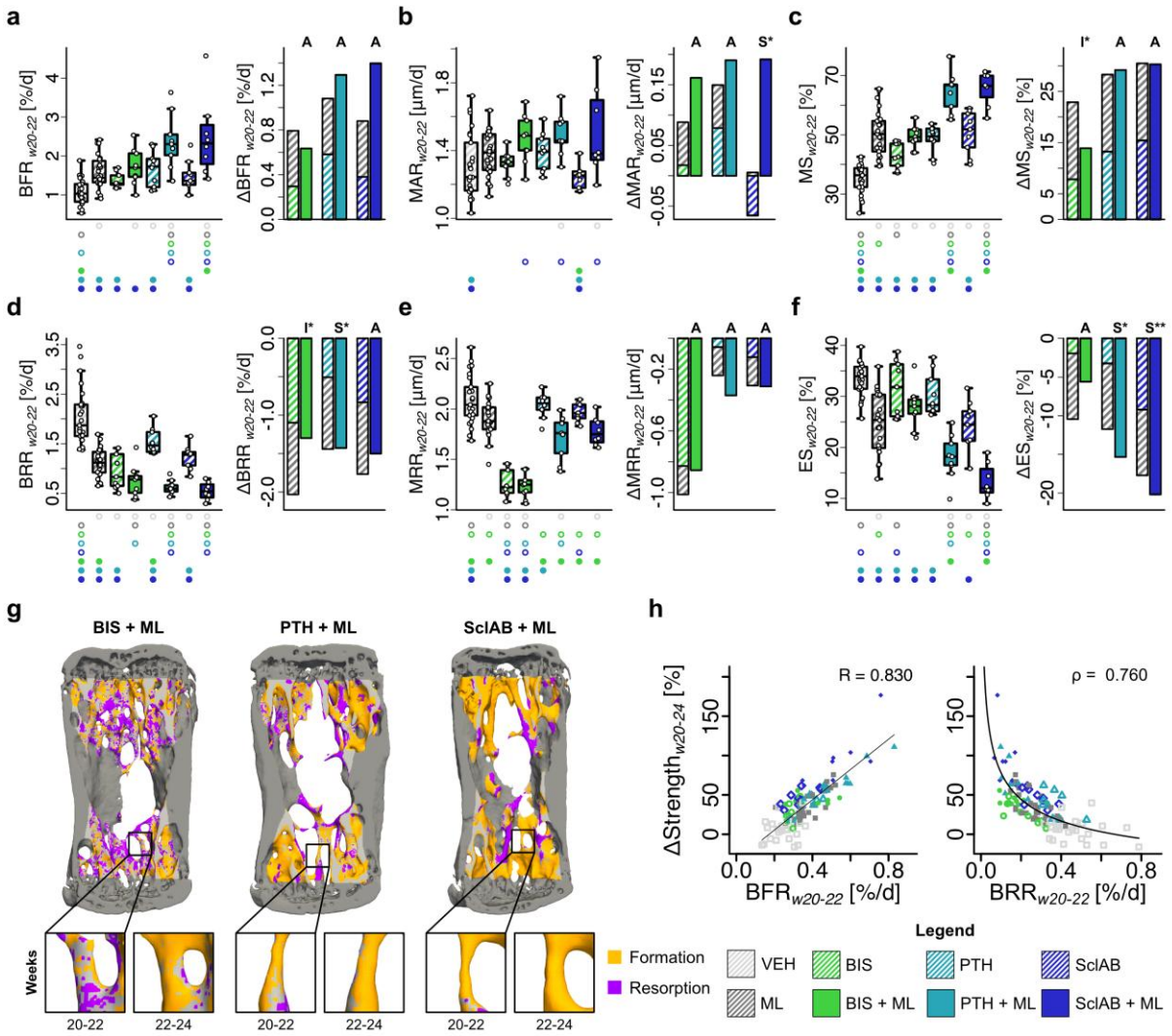

***Figure 3**: **Mechanical loading increases bone formation and decreases resorption rates of anabolic and anti-catabolic pharmacological treatments which contribute to increased predicted strength.** (**a**) bone formation rate per bone volume (BFR) (**b**) mineral apposition rate (MAR) (**c**) mineralizing surface per bone surface (MS) (**d**) bone resorption rate per bone volume (BRR) (**e**) mineral resorption rate (MRR) (**f**) eroded surface per bone surface (ES). **(a-f)** The box spans the interquartile range (IQR) from the 25th to the 75th percentile. The median is shown as a line inside the box. Whiskers extend to the most extreme data points within 1.5 × IQR, points beyond this range are plotted as outliers. Δ denotes difference from VEH as no baseline value for dynamic bone morphometry rates was available. Bars show group means of sum of single vs. combined treatment indicating: antagonistic (I), additive (A) or synergistic (S) effects determined via treatment:loading interaction in a linear model on the log_2-transformed values. Significances were calculated using ANOVA followed by Tukey's post-hoc test; significant differences are depicted with a symbol in the color of the corresponding group (o: to monotreatment, ●: to combined treatment,* see Supplementary Table S.1 for color encoding, $p<0.05$). (**g**) Visual representations of combination groups BIS + ML, PTH + ML, and SclAB + ML in week intervals w20-22 and w22-24 (**h**) Linear regression of ΔStrength with BFR, and exponential regression analysis with BRR in week interval w20-22.*

Bone formation and resorption occur in mechanically distinct strain windows

To address the question whether pharmacological treatments target bone (re)modeling to the places that mechanically need it, we correlated the underlying mechanical signals in the trabecular compartment with subsequent formation and resorption events. Visually, spatial agreement was found between high SED and regions of subsequent bone formation, and low SED and regions of subsequent bone resorption (Fig. 4a). Quantitative analysis (Fig. 4b) showed that mean SED was significantly higher at formation sites ($p<0.05$) and significantly lower at resorption sites ($p<0.05$) compared to quiescent surfaces, when expressed relative to the average quiescent SED across all animals per group. The addition of mechanical loading to the monotreatments resulted in marginal changes, indicating that bone formation and resorption continue to occur in mechanically distinct strain windows despite possible influences of pharmacological interventions. Levene's test revealed significantly smaller variances between BIS and BIS + ML and between VEH and ML ($p<0.05$), indicative of more consistent mechanosensitive responses in these groups in the presence of mechanical loading.

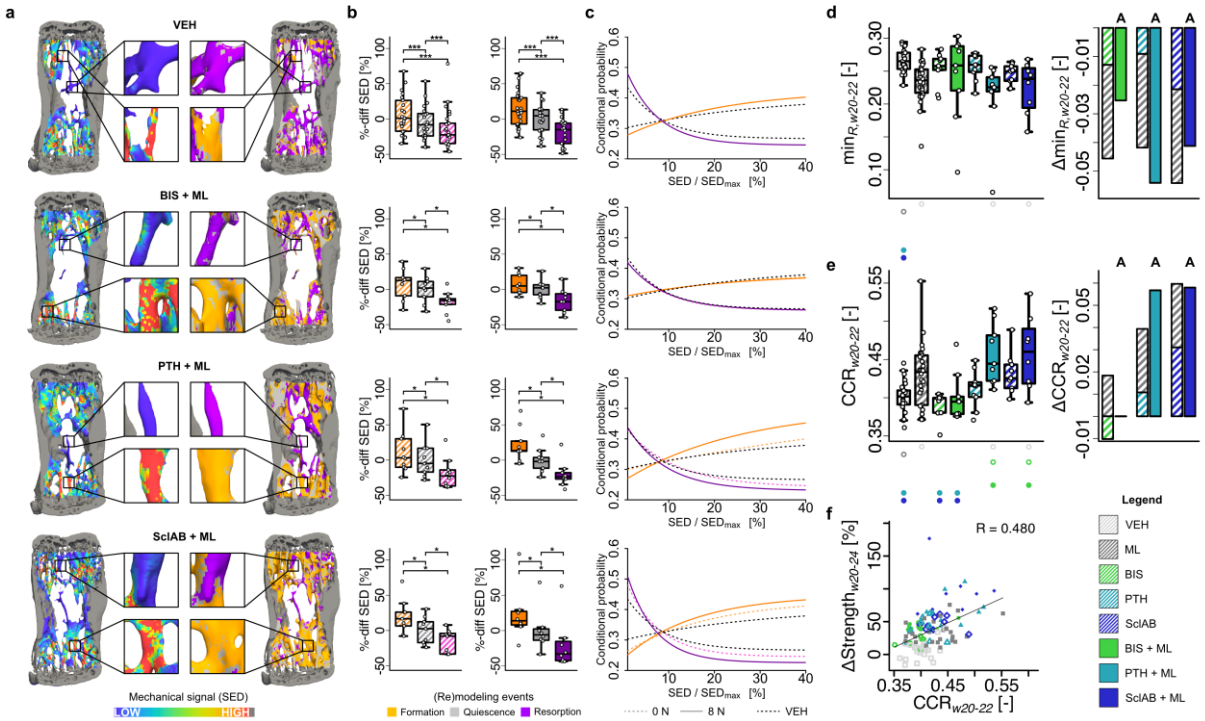

***Figure 4: Formation aligns with high mechanical signal, resorption with low**: **(a)** Spatial comparison of local mechanical signal (SED at week 20) with sites of trabecular bone formation and resorption (w20-22). **(b)** SED at formation, resorption, and quiescent sites[6], normalized to the group mean of quiescence to allow statistical testing with this group. The box spans the interquartile range (IQR) from the 25th to the 75th percentile. The median is shown as a line inside the box. Whiskers extend to the most extreme data points within 1.5 × IQR, points beyond this range are plotted as outliers. *p<0.05, ***<0.001 using two-sided paired Wilcoxon-signed rank test with Bonferroni correction. **(c)** Conditional probabilities of formation and resorption as a function of SED. VEH indicated by black dotted line. Values are cropped above 40% due to* low voxel count[6]. ***(d)** Asymptotic resorption probability value (min_R). Δ denotes change from VEH; sum of single vs. combined treatment group means indicating antagonistic (I), additive (A) or synergistic (S) effects **(e)** CCR as a measure of mechanoregulated (re)modeling **(f)** Linear regression analysis in interval 20-22 of ΔStrength with CCR. Significant differences are depicted with a symbol in the color of the corresponding group (o: to monotreatment, ●: to combined treatment,* see Supplementary Table S.1 for color encoding, *p<0.05).*

Conditional probabilities of formation, quiescence, and resorption events for a given SED-value were calculated and fitted with exponential functions. The probability for bone formation increased with increasing SED, and the probability for bone resorption decreased with increasing SED (Fig. 4c, Supplementary Fig. S.3 and Table S.6 for results in w22-24). Especially the PTH + ML and SclAB + ML conditional probability curves opened up compared to their monotreatments, indicating a higher responsiveness to mechanical signals (Fig. 4c). The asymptotic resorption probability value min_R, which can be interpreted as the basal level of resorption independent from the mechanical signal, was significantly lower in ML, PTH + ML, and in SclAB + ML than in VEH ($p<0.05$, Fig. 4d, Table S.8). Further comparisons of the coefficients from fitted functions to the conditional probabilities are provided in Supplementary Tables S.7 and S.8. The presence of few significant differences between groups suggests mechanosensitivity of the system is largely preserved regardless of the presence or absence of mechanical loading. Combined anabolic treatments resulted in higher correct classification rate (CCR) values compared to VEH and the BIS groups (Fig. 4e), with CCR being a metric used to evaluate the accuracy of classifying local bone formation or resorption events based on predicted mechanical signals. However, CCR only correlated moderately with the increases in

strength, indicating increased mechanosensitivity of the system may not fully explain the ability of bone to increase strength (Fig. 4f).

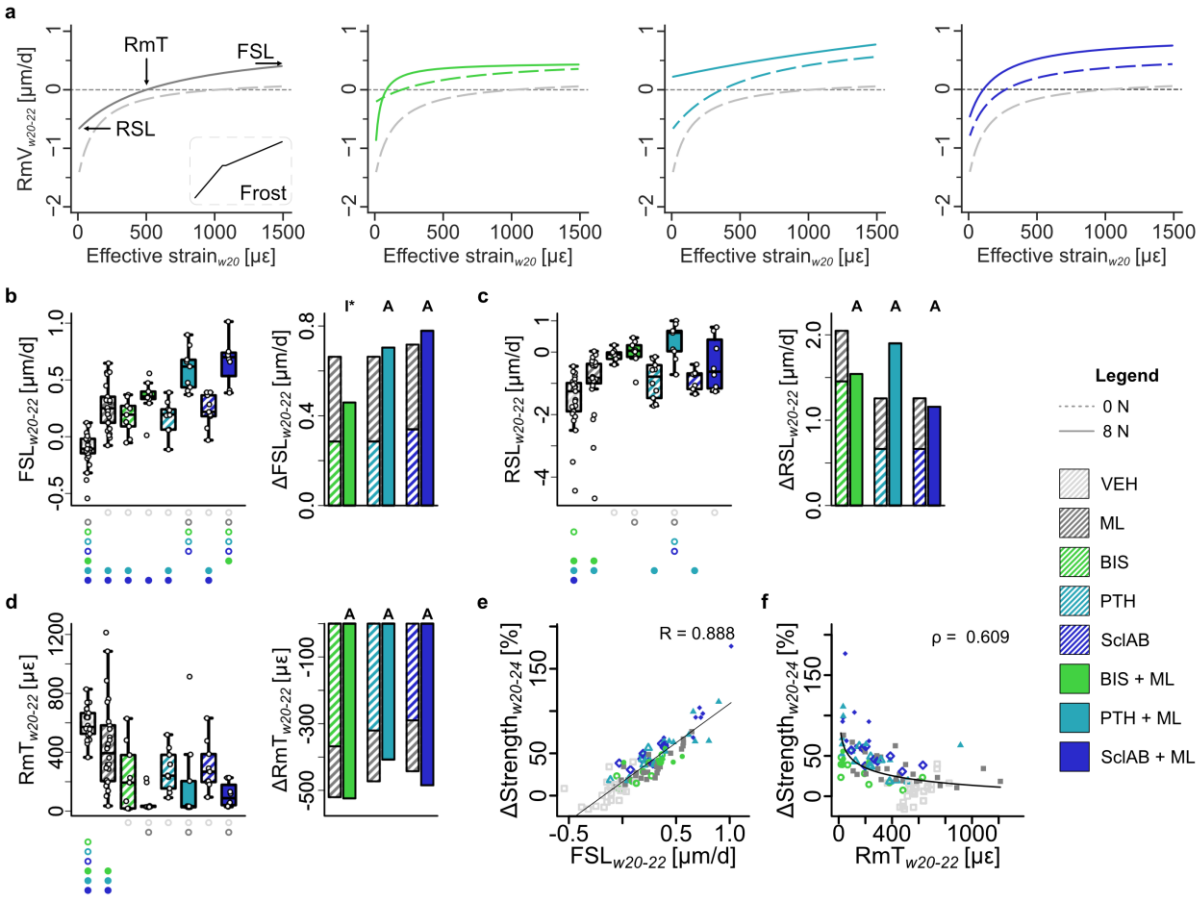

Figure 5: (Re)modeling velocity curves as an approximation of the mechanostat theory. (a) *(re)modeling velocity (RmV) curves for VEH / ML, BIS / BIS + ML, PTH / PTH + ML, SclAB / SclAB + ML; (b) formation saturation level (FSL) (c) resorption saturation level (RSL), (d) (re)modeling threshold (RmT)* ***(b-d)****: The box spans the interquartile range (IQR) from the 25th to the 75th percentile. The median is shown as a line inside the box. Whiskers extend to the most extreme data points within 1.5 × IQR, points beyond this range are plotted as outliers. Δ denotes difference from VEH as no baseline value from week 20 was available. Bars show group means of sum of single vs. combined treatment indicating: antagonistic (I), additive (A) or synergistic (S) effects determined via treatment:loading interaction in a linear model on the absolute values. Significances were calculated using ANOVA followed by Tukey's post-hoc test; significant differences are depicted with a symbol in the color of the corresponding group (o: to monotreatment, ●: to combined treatment,* see Supplementary Table S.1 for color encoding, *p<0.05). (**g**) Linear regression of ΔStrength with FSL, and power-law regression analysis with RmT from week interval w20-22.*

289

290 **Frost's mechanostat setpoints are shifted towards lower values for mono- and combined**
291 **treatments**

292 To assess potential shifts in the setpoints due to different drug or combination treatments,
293 (re)modeling velocity (RmV) curves and mechanostat parameters[19] were calculated for each
294 treatment group as an approximation to the mechanostat theory. These curves show the net
295 RmV for a given surface effective strain, where a negative value means net resorption and a
296 positive value means net formation (Fig. 5a). From these curves, formation saturation levels
297 (FSL), resorption saturation levels (RSL), and (re)modeling thresholds (RmTs) were derived.

298 FSL was increased in all treatments compared to VEH ($p<0.001$, Fig. 5b, Supplementary Table
299 S.9), and was significantly higher in anabolic combination groups compared to the respective
300 monotreatments ($p<0.001$). This suggests an increased mechanosensitivity of the cells involved
301 in bone formation. RSL was increased in the BIS and all combination groups compared to VEH
302 ($p<0.05$, Fig. 5c). The increase in RSL under bisphosphonate treatment may be explained by
303 the suppression of bone turnover: at comparable strain levels, resorption would typically occur,
304 resulting in a lower RSL; however, due to inhibited osteoclast activity, this resorptive response
305 is blunted, making the system appear saturated at a higher RSL value. Regarding the role of
306 additional mechanical loading, only the PTH + ML group showed a significant increase
307 compared to PTH alone ($p<0.05$, Supplementary Table S.9). This suggests that, under strain
308 conditions that would typically lead to bone resorption, the balance has shifted towards bone
309 formation. RmT values, representing the setpoints in the mechanostat theory, were decreased
310 in all pharmacological treatment groups compared to VEH ($p<0.05$), with no significant
311 improvements observed in the combination groups receiving mechanical loading (Fig. 5d).
312 These results were even more pronounced in the second time interval (Supplementary Fig. 4d,
313 Table S.9). The reduction in RmT suggests an upregulation of osteocytic mechanosensitivity,

314 an expected outcome in the anabolic treatment groups, but an unexpected finding in the
315 bisphosphonate-treated groups. This may reflect a compensatory osteocytic response to the
316 suppressed bone resorption induced by bisphosphonate treatment. Furthermore, FSL correlated
317 strongly with predicted strength increases ($R = 0.888$), while RmT exhibited a moderate inverse
318 correlation ($\rho = 0.609$) when fitted with a power-law function. These findings suggest that a
319 reduction in RmT may be a prerequisite for strength gains; however, actual increases in strength
320 require anabolic potential (Fig. 5e,f).

321

322 **The amount of modeling correlates highly with increases in predicted strength for all**
323 **treatments**

324 Next, we distinguished between the remodeling and the modeling ability of the different
325 treatments. Visually, in several areas in VEH, high SED values decreased over time, but in
326 other areas they increased and the resorption of a single trabecula led to a more heterogeneous
327 SED distribution (Fig. 6a). While SED on average decreased over time for BIS + ML, this did
328 not particularly affect areas with high SED, as there remained several highly strained areas in
329 week 24. In contrast, both PTH + ML and SclAB + ML showed large decreases in SED,
330 especially in areas with high SED values in week 20 (Fig. 6a).

331 The remodeling ability - as represented by the amount of resorption followed by formation -
332 was in BIS, BIS + ML, PTH and SclAB comparable to VEH, and significantly lower in ML
333 and the anabolic combination groups compared to VEH ($p<0.05$, Fig. 6b). In contrast, the
334 modeling ability was significantly higher compared to VEH in all but the BIS group, with the
335 highest amount in the anabolic combination treatments ($p<0.001$, Fig. 6c). Both remodeling and
336 modeling capacity showed antagonistic effects in BIS + ML and additive effects in anabolic
337 combination treatments (Fig. 6b,c). Remodeling showed a moderate inverse correlation with
338 increases in predicted strength when fitted with a power-law function ($\rho = 0.476$, Fig. 6d), while

339 modeling correlated strongly in a linear fit (R = 0.928, Fig. 6e). Fig. 6f illustrates the distribution
340 of surface events relative to increasing effective strain. Remodeling events appeared strain-
341 independent, and modeling increased with higher mechanical stimuli, particularly in the
342 anabolic combination groups (Fig. 6f). There is also a non-linear increase in modeling with
343 mechanical loading in comparison to the mono-treatment, with a stronger effect for low
344 effective strain regions, especially for SclAB. Fig. 6g summarizes the trabecular bone response
345 across treatments. Bisphosphonates, alone or with mechanical loading, help preserve trabecular
346 interconnectedness. Anabolic treatments combined with mechanical loading effectively
347 enhance predicted strength by promoting formation and suppressing resorption. These additive
348 effects across parameters likely underlie the observed synergistic gains in predicted strength, at
349 least in SclAB.

350

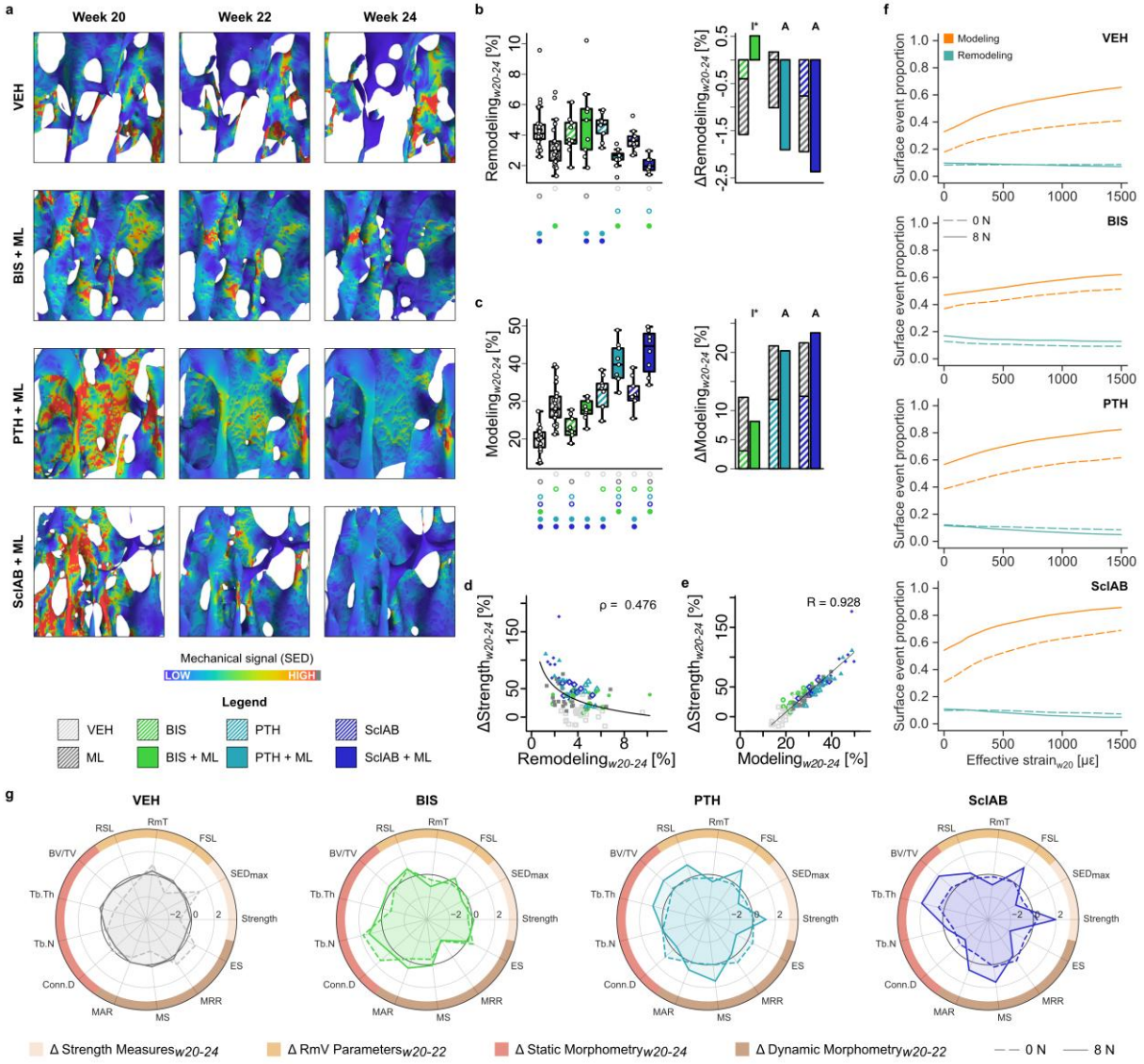

Figure 6: Modeling capacity correlates highly with the increase in predicted strength. (a) *Heterogeneity of the strain distribution decreases to different extents in different treatments. Qualitative comparison of changing SED-distribution for VEH, BIS + ML, PTH + ML and ScIAB + ML over the course of 4 weeks of treatment.* ***(b)*** *Remodeling as calculated from formation following resorption at the same location over 3 measurement time points (w20, w22, w24).* ***(c)*** *Modeling as calculated from formation following quiescence at the same location over 3 measurement time points (w20, w22, w24)* ***(b-c)****: The box spans the interquartile range (IQR) from the 25th to the 75th percentile. The median is shown as a line inside the box. Whiskers extend to the most extreme data points within 1.5 × IQR, points beyond this range are plotted as outliers. Δ denotes change from VEH; sum of single vs. combined treatment group means indicating graphically antagonistic (I), additive (A) or synergistic (S) effects. Significant differences are depicted with a symbol in the color of the corresponding group (o: to monotreatment, ●: to combined treatment,* see Supplementary Table S.1 for color encoding, *p<0.05).* ***(d)*** *Remodeling amount in % correlated to increases in predicted strength fitted using a power-law function.* ***(e)*** *Modeling amount in % correlated to increases in predicted strength fitted using linear regression.* ***(f)*** *Surface event proportion (modeling or remodeling) in relation*

to the mechanical signal. ***(g)*** *Spider plots summarizing the mean of outcome parameters of the analyzed treatments. Values were standardized to facilitate visual comparisons between groups.*

Discussion

The main goal of osteoporosis therapy is to restore bone mass to reduce fracture risk. To achieve this efficiently, existing bone must be preserved and new bone formed at mechanically relevant sites. In healthy bone, bone (re)modeling is proposed to be regulated via the mechanostat[6,19-21]. Here, we investigated how three current pharmacological treatments influence this regulation in the initial treatment phases in osteoporotic mice, particularly when combined with mechanical loading. Our findings suggest that all three investigated treatments induce bone formation and inhibit bone resorption at the mechanically relevant sites, but it was only in anabolic therapies that mechanical loading additively (PTH) or synergistically (SclAB) enhanced predicted bone strength.

When combined with sclerostin antibody treatment, mechanical loading led to a synergistic increase in predicted bone strength and an additive increase in bone volume fraction. Mineral apposition rates and reductions in eroded surfaces were synergistic, consistent with previous findings[12,22,23]. This response may be explained by dual suppression of the activity of sclerostin, a protein secreted by osteocytes that antagonizes Wnt signaling[11]. While mechanical loading independently suppresses sclerostin expression in osteocytes[13], SclAB pharmacologically neutralizes any residual sclerostin[11]. Together, these effects enhance Wnt/β-catenin activity, and likely contribute to the pronounced anabolic response[24]. Additional pathways may also be involved, as suggested by studies in SOST-KO mice, which still showed loading-induced bone formation[25]. One candidate is Dickkopf-1 (Dkk1), another Wnt inhibitor[26-28]. Robling et al.[13] reported that mechanical loading reduced both *Sost* mRNA (-73%) and *Dkk1* (-49%) transcripts. Since both proteins compete at LRP5/6 receptors in osteoblasts and osteocytes, their

389 simultaneous inhibition may underlie the observed synergy between SclAB and mechanical
390 loading.

391 We found additive increases in predicted strength and increased sensitivity of
392 mechanoregulation mechanisms for PTH + ML, which is in line with previous results where
393 PTH increased the mechanoresponse of osteoblasts only when combined with fluid flow[29].
394 Hagino et al.[30] hypothesized that PTH lowers the (re)modeling threshold of the (re)modeling
395 velocity function, which our findings support (Fig. 5). In previous animal studies, mechanical
396 loading combined with intermittent PTH (1-34) treatment led to synergistic effects in the
397 trabecular compartment of the healthy tibia, but it was only prevalent in regions that were not
398 remodeled, but modeled[31].

399 Bisphosphonates were the only treatment that preserved Tb.N but showed no additive effects
400 with mechanical loading, consistent with clinical[32 33] studies reporting limited benefit of
401 combining bisphosphonates and exercise[32 33]. Since mineralizing surface was significantly
402 increased in the bisphosphonate group compared to the vehicle group, our results suggest that
403 bisphosphonates not only affect the activity of osteoclasts but also that of osteoblasts, possibly
404 through disruption of the coupling process via elevated osteoclast apoptosis[34], potentially
405 impairing the spatial guidance of osteoblasts by the mechanical signal. The observation that the
406 BIS and BIS+ML groups exhibit RmT values as low as other treatment groups despite showing
407 the least overall remodeling response may indicate a compensatory increase in osteocytic
408 mechanosensitivity, potentially allowing selective resorption of mechanically less relevant
409 areas.

410 This study focuses on osteoblast and osteoclast surface activities using *in vivo* micro-CT, which
411 allows longitudinal tracking of bone (re)modeling. Histological analysis could offer further
412 insight into cellular and tissue-level mechanisms to support the cell-specific interpretations
413 derived from the micro-CT data. However, due to the method of tissue preservation and the

limited number of available samples, it was not considered feasible in the current study. It's worth noting though that previous work demonstrated a significant correlation between micro-CT-derived and histomorphometry-based MS and MAR ($R \approx 0.59 - 0.78$)[35,36]. Furthermore, Birkhold et al.[37] have demonstrated the ability of longitudinal *in vivo* micro-CT to reliably quantify bone (re)modeling, i.e. separation into modeling and remodeling, in both trabecular and cortical bone. While *in vivo* micro-CT does not allow direct visualization of osteocytes, our measurements reflect the functional output of the bone cells in which osteocytes play an important role through orchestration of bone formation and resorption in response to local mechanical stimuli[6].

Regions with high local strain are linked to higher occurrences of microscopic tissue damage[38] of which even small amounts can lead to large reductions in strength[39] and increase fracture risk[40]. Reductions in strain energy density (SED) over time do not necessarily imply a decrease in bone formation capacity but rather reflect system saturation, consistent with mechanostat theory, where bone formation plateaus once strain thresholds are reached.

As a limitation, our developed system does not yet incorporate the level of the transcriptome[41]. Other cell types, particularly immune cells and endothelial cells, also contribute to bone (re)modeling via inflammatory signaling and vascularization, respectively. Recent work originating from fracture healing highlights the role of immune and vascular interactions, particularly in the context of aging and mechanical loading[42]. While these cell types were not analyzed here, future multimodal approaches could complement imaging-based assessments.

Given the biological differences among the therapies selected, including administration routes and duration limitations, direct long-term comparisons are not the aim of this study. Instead, our focus on short-term effects aimed to investigate potential synergistic improvements in bone strength and to gain mechanistic insight into how pharmacological and mechanical stimuli modulate mechanoregulation. The findings support mechanostat theory: treatments lower

439 mechanical setpoints, enabling bone formation at lower strains. However, only anabolic
440 treatments effectively reinforce highly loaded trabeculae and reduce peak strains, underscoring
441 the importance of modeling capacity for strength gains. And while our results highlight the
442 promise of mechanical loading as an adjunct to anabolic therapies, clinical studies will
443 ultimately be required to determine optimal exercise modalities, just as pharmacological dosing
444 requires careful optimization.

445 In conclusion, the current study revealed that drug treatments target trabecular bone
446 (re)modeling at mechano-functionally relevant places, and osteoanabolic treatments in
447 combination with mechanical loading additively and synergistically increased the bone
448 response. The additive (PTH) and synergistic (SclAB) increases in predicted strength can be
449 explained by reductions in resorption rates, shifts in the (re)modeling thresholds as described
450 by Frost in the mechanostat theory more than 30 years ago, and by the modeling ability of
451 anabolic treatments. Being able to link organ-level changes induced by physical or
452 pharmacological therapies to the mechanosensitivity of the cells provides information on how
453 well skeletal structures can adapt to mechanical demands under pathological or treatment
454 conditions, a task for which the body has optimized itself over millions of years of evolution.
455 Load-bearing exercise may represent a promising adjunct option for physically active
456 osteoporosis patients on osteoanabolic therapy.

457

458 # Methods

459 **Study design**

460 The study design is illustrated in Fig. 1a. In total, 120 female 15-week-old C57BL/6 mice
461 (n=60, C57BL/6JRccHsd, RCC/Harlan; Füllinsdorf, Switzerland/ Horst, The Netherlands;
462 n=60, C57BL/6JRj mice (Janvier Labs, Le Genest-Saint-Isle, France) were subjected to

463 bilateral ovariectomy. A basal micro-CT image of the 6th caudal vertebra was obtained (vivaCT
464 40, Scanco Medical, Brüttisellen, Switzerland). Recovery lasted five weeks after surgery, as in
465 this period, an osteopenic state was established in the trabecular compartment of the 6th caudal
466 vertebra in a previous study[43]. Pinning of the adjacent vertebrae as preparation for the loading
467 procedure took place in week 17. At week 20, the animals were divided into 8 groups and the
468 following treatments were administered for the following four weeks: BIS (n=9), BIS + ML
469 (n=9), PTH (n=10), PTH + ML (n=9), SclAB (n=9), SclAB + ML (n=8), ML (n=26), VEH
470 (n=25). 10 mice were excluded due to swollen tails or loose pins. In the SclAB study, 4 mice
471 showed a periosteal reaction, possibly due to injury of the periosteum during intravenous
472 injection at the tail vein. One mouse in the BIS + ML group did not lose bone volume after
473 ovariectomy. These mice were excluded from evaluation, resulting in 105 animals included.
474 Micro-CT was performed in weeks 15, 20, 22 and 24. Surgeries, imaging, and loading were
475 performed under isoflurane anesthesia (induction 4%, maintenance 1.5-2.5%, Attane, Piramal
476 Healthcare, India). Vehicle control was an isotonic buffer (pH 5.3). While the data was gained
477 in four experiments (at different times), study and loading parameters were not different except
478 for the administered pharmacological treatments, thus combined in this study. The bone
479 responses of the VEH and the ML groups of both mouse lines (JRccHsd and 6JRj) showed no
480 differences in reactions ($\Delta BV/TV_{w20-24;}$ VEH: $p = 0.937$; ML: $p = 0.206$; two-way ANOVA
481 followed by Tukey's post-hoc test), thus ML groups from all experiments and VEH groups
482 from all experiments were merged, explaining the larger sample size in these groups. The
483 merging was conducted because separate vehicle group presentations would not have yielded
484 additional insights but substantially would have increased data complexity (see Supplementary
485 Table S.3). All animal experiments were performed with approval of the local authority
486 (Kantonales Veterinäramt Zürich, Zurich, Switzerland, license number 171/2008, 108/2011,
487 078/2012).

488

489 **Mechanical loading**

490 A validated *in vivo* mouse tail loading model was used to induce trabecular bone adaptation
491 under controlled mechanical conditions[43-45]. Stainless steel pins were implanted into adjacent
492 vertebrae under fluoroscopic guidance three weeks prior to loading. An 8N cyclic axial load
493 (3000 cycles, 10 Hz) was applied to the 6th caudal vertebra (CV6) using a custom loading device
494 (caudal vertebra axial loading device, CVAD [44]) three times a week. Control animals (0N
495 groups) underwent identical procedures, including pin placement and anesthesia but no load
496 was applied. A force of 8 N was used in order to maximize the effect within a short timeframe.
497 It was the maximum force that could be applied based on what the pins within the bone could
498 bear, and represents twice the force exerted on mouse vertebrae under physiological
499 conditions[46]. No microdamage has been observed to date, although not systematically assessed
500 (unpublished data). In our experience, mechanical limitation arises at the pin sites due to
501 concentrated forces, not within the loaded vertebra. Pistoia simulations estimate a maximum
502 failure load of 24.5 N at CV6 in osteoporotic mice at week 20 (predicted trabecular strength,
503 see Table S.2).

504

505 **Pharmacological treatment**

506 The BIS group received 100 µg/kg zoledronate (Zometa 4 mg/5 ml; Novartis Pharma Schweiz
507 AG, Bern) subcutaneously once in week 20. Corresponding VEH (0.9% NaCl, B. Braun
508 Medical AG, Switzerland) was injected at the same time point. Mice in the PTH study received
509 40 µg/kg PTH (hPTH 1-34, Bachem AG, Switzerland) or the according VEH (0.9% NaCl)
510 subcutaneously daily over four weeks. SclAB (100 mg/kg, Novartis Pharma AG, Basel,
511 Switzerland) or the corresponding VEH (isotonic buffer, pH 5.3) was injected i.v. weekly into
512 the lateral tail vein over 4 weeks

513 BIS and SclAB doses were selected based on established protocols in the literature[24,47]. The
514 PTH dose was determined in a dose-response study comparing 10 µg/kg/d and 40 µg/kg/d,
515 following an initial 80 µg/kg/d dose proposed in the literature[48] that led to excessive increases
516 in bone volume fraction (BV/TV) by the end of the experiment. The 40 µg/kg/d dose was chosen
517 to obtain BV/TV increases comparable to those observed with BIS and SclAb treatments,
518 enabling a more balanced comparison across treatment groups (see Fig. 1b).

519

520 **Bone morphometry**

521 Micro-CT images were obtained with a vivaCT 40 (Scanco Medical AG, Brüttisellen,
522 Switzerland) operated at 55 kVp and 146 µA. 1000 projection images were obtained with an
523 integration time of 200 ms. Grayscale images were reconstructed using a Feldkamp algorithm,
524 with automated beam hardening correction, resulting in an isotropic voxel size of 10.5 µm. The
525 image of week 20 was aligned in the main loading direction. Follow up scans were registered
526 to the previous scan. A constrained 3D Gauss filter (sigma 1.2, support 1) and a global
527 thresholding procedure of 22% (approximately 580 mgHA/cm^3) were applied. Automated
528 masks were created to extract the trabecular bone volumes (trabecular mask truncated by 10%
529 of length at both ends to exclude epiphyses and primary spongiosa; middle 26% removed
530 because this area is almost void of trabeculae)[18]. The cortical mask included 75% of the length
531 of the inner mask[18]. Static trabecular bone morphometric parameters were calculated according
532 to Bouxsein et al.[49]. Dynamic bone morphometry was performed by registering and
533 superimposing segmented bone volume images of consecutive time points. Bone formation and
534 resorption rates were calculated as described previously[36] over two two-week periods (w20-22
535 and w22-24).

536

537 **Finite element analysis of mechanical properties**

538 Finite-element simulations were used to analyze mechanical properties of the vertebrae. 3D
539 micro-FE models were generated by converting all voxels of the micro-CT image to 8 node
540 hexahedral elements, with each model consisting of approximately 1.8 million elements. A
541 Young's modulus of 14.8 GPa and a Poisson's ratio of 0.3[44] were assigned. Each model was
542 solved with ParOSol[50] running on the Euler cluster operated by Scientific IT Services at ETH
543 Zurich. Cylindric intervertebral disks (10% of absolute height) were applied and assigned the
544 same Young's modulus and Poisson's ratio as bone. The top of the model was displaced by 1%
545 of the total vertebral length, while the bottom was fixed. The resulting reaction force was
546 rescaled to the value of the force applied in the experimental setup; consequently, all the FE
547 outcomes were rescaled accordingly (4 N for non-loaded[46] and 8 N for loaded mice). Strain
548 energy density (SED), defined as the increase in energy associated with the tissue deformation
549 per unit volume, and effective strain were used as the mechanical signal. Trabecular bone
550 strength was estimated for each mouse at each time point by using the Pistoia criterion[51] which
551 assumes that bone failure is initiated if a certain percentage of the bone tissue (2%) is strained
552 beyond the tissue yield effective strain (7000 με). This criterion has been shown applicable to
553 the mouse vertebra as well[52]. For the predicted bone strength estimation, the full bone was
554 modeled but only the effective strains in the trabecular compartment were analyzed.

555

556 **Local mechanoregulation analysis**

557 The local mechanical environment was derived from micro-FE simulations of the baseline scan.
558 Here, SED is used as a mathematical term to describe the (re)modeling stimulus
559 phenomenologically. To quantify the relationship between the local SED and cellular activity
560 on the bone surface, the bone formation or resorption sites determined by rigid registration were
561 projected onto the surface of the baseline scan, resulting in three masks representing three
562 different clusters of formed (F), quiescent (Q) or resorbed (R) bone, as described previously[6].

563 In short, the mean SED value was calculated in each of these three masks and for each mouse,
564 and normalized to the mean SED of the quiescent surface as absolute SED values differ per
565 mouse and over time due to differences in BV/TV. To establish a quantitative description of
566 the mechanoregulatory system, the relation between increasing mechanical stimuli and
567 consequent (re)modeling events was assessed by calculating the relative percentage of voxels
568 being formed, quiescent and resorbed for each value of SED binned at 1% step size of the
569 maximum SED, and assuming that each (re)modeling event has the same occurrence probability
570 (i.e., formation, resorption and quiescent regions were virtually rescaled to have the same
571 amount of voxels) to remove dependencies on imbalances in the (re)modeling process due to
572 differences between animals or treatments. The conditional probabilities were fitted per animal
573 by exponential functions. Correct classification rate (CCR) values were calculated from the
574 mean conditional probabilities from all animals, returning a scalar value between 0.33 and 1
575 assessing overall mechanoregulation, with 0.33 meaning (re)modeling is independent of the
576 mechanical signal and 1 meaning it is entirely dependent on the mechanical signal.
577 (Re)modeling velocities (RmVs) and their mechanostat parameters were calculated according
578 to Marques et al. for each animal[19]. Minimum and maximum RmV, represented as formation
579 saturation level (FSL) and resorption saturation level (RSL), as well as (re)modeling thresholds
580 (RmTs) were extracted from the resulting curves.

581

582 **Statistical methods**

583 Statistical analysis was performed using R (R, Auckland, New Zealand[53]). Data are presented
584 as mean ± standard error unless otherwise specified. P-values lower than 0.05 are considered
585 significant, statistical significance was defined as *$p<0.05$, **$p<0.01$, ***$p<0.001$. Normality
586 was assessed using the Shapiro–Wilk test (in R, with $\alpha = 0.05$).

Static morphometric and mechanical parameters of trabecular bone in the 6th caudal vertebra were measured at weeks 15, 20, 22, and 24, with Δ representing the percentage change between weeks 20 and 24. ANOVA followed by Tukey's post-hoc test was used to compare Δw20-24. Synergy (S) or antagonism (I) between treatment and mechanical loading was evaluated using the interaction term ("treatment:mechanical loading") in a linear model.

A synergistic effect was defined as a combined treatment response that exceeded the sum of the individual effects of treatment and mechanical loading. This implies that the two interventions may act through the same or facilitating biological pathways. Statistically, such synergy is indicated by a significant and positive interaction term between the main effect (treatment) and mechanical loading. An antagonistic effect was defined as a combined treatment response that was less than the expected additive effect of treatment and mechanical loading. Statistically, such antagonism was reflected by a significant and negative interaction term between the main effect (treatment) and mechanical loading. The animal provider from the third (SclAB) and fourth (PTH) experiment was different, therefore we adjusted the model for this.

Dynamic morphometric parameters were analyzed during weeks 20-22 and 22-24. ANOVA followed by Tukey's post-hoc test was applied to absolute values in each time interval. Synergy or antagonism was assessed using the interaction term from a linear model of $\log_2$-transformed values in each time interval.

Strain Energy Density (SED) in formation (F), quiescence (Q), and resorption (R) surfaces was reported for each group in each time interval. Differences between F, Q, and R were compared using two-sided Wilcoxon signed-rank tests with Bonferroni correction after testing for normality.

For conditional probabilities, exponential curves were fitted to the formation and resorption slopes. For formation, a saturating exponential model $f(x) = y_0 + a \cdot (1 - \exp(-bx))$ was applied to the first 40% of normalized SED data, with parameters y_0, a, and b representing

baseline, maximal formation, and sensitivity to mechanical stimulus, respectively. For resorption, a decaying exponential model $f(x) = y_0 + a \cdot \exp(-bx))$ was used to assess the rate of resorption. Synergy or antagonism was assessed using the interaction term from a linear model applied to $\log_2$-transformed coefficients, with significance determined by ANOVA followed by Tukey's post-hoc test.

Formation and resorption saturation levels (FSL, RSL) and remodeling thresholds (RmTs) were derived from hyperbola remodeling velocity curves, fitted with the function $f(x) = y_0 + \frac{a}{(b-x)}$, where x represents the mechanical signal, y_0 the FSL, and a the (re)modeling velocity modulus. The remodeling threshold (RmT) is defined as: $RmT = b + \frac{a}{y_0}$. ANOVA followed by Tukey's post-hoc test was used for statistical comparisons, with synergy or antagonism assessed using the interaction term from a linear model applied to absolute values in each time interval, because FSL and RSL can obtain negative values.

Linear correlations between the %-change in predicted strength and parameter outcomes were assessed using Pearson's correlation coefficient R. For nonlinear relationships, we employed a power-law model of the form $y = a \cdot x^b$, which was linearized via logarithmic transformation to $\ln(\mathrm{y}) = \ln(a) + b \cdot \ln(x)$. Parameters a and b were estimated using linear regression on the transformed data, and the Spearman's correlation coefficient ρ between the log-transformed observed and predicted values was used to assess the goodness of fit.

Acknowledgments

We acknowledge Kathleen Koch for assistance and performance of animal experiments of the PTH and BIS groups, and Dr. Ulrike Kettenberger for assistance and performance of animal experiments of the PTH group. Nirujan Pasupathy and Júlia van den Nest Molina have supported the analyses of modeling and mechanoregulation mechanisms. This work was

funded by the European Union grant VPHOP (FP7-ICT-2008-223865) and the European Research Council ERC Advanced grant (MechAGE ERC-2016-ADG-741883).

Author contributions

RM, GAK, PJR designed the experiment. CW, GAK, MS, FML performed the experiment. FAS, FCM, JG, CW, MS, FML, GAK performed image processing and analysis. MK provided pharmacological agents. RM, GAK, PJR, CK supervised the project. FAS wrote the original draft of the manuscript. All authors contributed to data interpretation, were involved in discussions throughout the study, and participated in manuscript revision and preparation.

Ethics declarations

Competing interests

MK, PJR, and CK are employees of Novartis. The other authors declare they have no competing interests.

References

1. Kanis, J.A., *et al.* A reference standard for the description of osteoporosis. *Bone* **42**, 467-475 (2008).
2. Schumm, A.K., *et al.* Does adding exercise or physical activity to pharmacological osteoporosis therapy in patients with increased fracture risk improve bone mineral density and lower fracture risk? A systematic review and meta-analysis. *Osteoporosis Int* **34**, 1867-1880 (2023).
3. Kim, S.W., *et al.* Sclerostin Antibody Administration Converts Bone Lining Cells Into Active Osteoblasts. *Journal of Bone and Mineral Research* **32**, 892-901 (2017).
4. Duan, P. & Bonewald, L.F. The role of the wnt/beta-catenin signaling pathway in formation and maintenance of bone and teeth. *Int J Biochem Cell Biol* **77**, 23-29 (2016).
5. Kim, J.M., Lin, C., Stavre, Z., Greenblatt, M.B. & Shim, J.H. Osteoblast-Osteoclast Communication and Bone Homeostasis. *Cells* **9**(2020).
6. Schulte, F.A., *et al.* Local mechanical stimuli regulate bone formation and resorption in mice at the tissue level. *PLoS One* **8**, e62172 (2013).
7. Dell, R.M., *et al.* Incidence of atypical nontraumatic diaphyseal fractures of the femur. *J Bone Miner Res* **27**, 2544-2550 (2012).

8. Kulkarni, N.H., *et al.* Effects of parathyroid hormone on Wnt signaling pathway in bone. *J Cell Biochem* **95**, 1178-1190 (2005).
9. Sugiyama, T., *et al.* Mechanical loading enhances the anabolic effects of intermittent parathyroid hormone (1-34) on trabecular and cortical bone in mice. *Bone* **43**, 238-248 (2008).
10. Rooney, A.M., McNeill, T.J., Ross, F.P., Bostrom, M.P.G. & van der Meulen, M.C.H. PTH Treatment Increases Cortical Bone Mass More in Response to Compression than Tension in Mice. *Journal of Bone and Mineral Research* **38**, 59-69 (2023).
11. Baron, R. & Kneissel, M. WNT signaling in bone homeostasis and disease: from human mutations to treatments. *Nat Med* **19**, 179-192 (2013).
12. Ominsky, M.S., Boyce, R.W., Li, X. & Ke, H.Z. Effects of sclerostin antibodies in animal models of osteoporosis. *Bone* **96**, 63-75 (2017).
13. Robling, A.G., *et al.* Mechanical stimulation of bone in vivo reduces osteocyte expression of Sost/sclerostin. *J Biol Chem* **283**, 5866-5875 (2008).
14. Rauner, M., Taipaleenmaki, H., Tsourdi, E. & Winter, E.M. Osteoporosis Treatment with Anti-Sclerostin Antibodies-Mechanisms of Action and Clinical Application. *J Clin Med* **10**(2021).
15. Frost, H.M. The mechanostat: a proposed pathogenic mechanism of osteoporoses and the bone mass effects of mechanical and nonmechanical agents. *Bone Miner* **2**, 73-85 (1987).
16. Frost, H.M. Bone "mass" and the "mechanostat": a proposal. *Anat Rec* **219**, 1-9 (1987).
17. Frost, H.M. Bone's mechanostat: a 2003 update. *Anat Rec A Discov Mol Cell Evol Biol* **275**, 1081-1101 (2003).
18. Lambers, F.M., Schulte, F.A., Kuhn, G., Webster, D.J. & Muller, R. Mouse tail vertebrae adapt to cyclic mechanical loading by increasing bone formation rate and decreasing bone resorption rate as shown by time-lapsed in vivo imaging of dynamic bone morphometry. *Bone* **49**, 1340-1350 (2011).
19. Marques, F.C., *et al.* Mechanostat parameters estimated from time-lapsed micro-computed tomography data of mechanically driven bone adaptation are logarithmically dependent on loading frequency. *Front Bioeng Biotech* **11**(2023).
20. Christen, P., *et al.* Bone remodelling in humans is load-driven but not lazy. *Nat Commun* **5**, 4855 (2014).
21. Griesbach, J.K., Schulte, F.A., Schadli, G.N., Rubert, M. & Muller, R. Mechanoregulation analysis of bone formation in tissue engineered constructs requires a volumetric method using time-lapsed micro-computed tomography. *Acta Biomater* (2024).
22. Taylor, S., *et al.* Time-dependent cellular and transcriptional changes in the osteoblast lineage associated with sclerostin antibody treatment in ovariectomized rats. *Bone* **84**, 148-159 (2016).
23. Ominsky, M.S., *et al.* Romosozumab Improves Bone Mass and Strength While Maintaining Bone Quality in Ovariectomized Cynomolgus Monkeys. *Journal of Bone and Mineral Research* **32**, 788-801 (2017).
24. Morse, A., *et al.* Sclerostin Antibody Augments the Anabolic Bone Formation Response in a Mouse Model of Mechanical Tibial Loading. *J Bone Miner Res* **33**, 486-498 (2018).
25. Morse, A., *et al.* Mechanical load increases in bone formation via a sclerostin-independent pathway. *J Bone Miner Res* **29**, 2456-2467 (2014).
26. Witcher, P.C., *et al.* Sclerostin neutralization unleashes the osteoanabolic effects of Dkk1 inhibition. *Jci Insight* **3**(2018).
27. Morse, A., *et al.* KO Mice Treated with Sclerostin Antibody Have Additional Increases in Bone Volume. *Calcified Tissue Int* **103**, 298-310 (2018).
28. Florio, M., *et al.* A bispecific antibody targeting sclerostin and DKK-1 promotes bone mass accrual and fracture repair. *Nature Communications* **7**(2016).
29. Ryder, K.D. & Duncan, R.L. Parathyroid hormone modulates the response of osteoblast-like cells to mechanical stimulation. *Calcif Tissue Int* **67**, 241-246 (2000).
30. Hagino, H., Okano, T., Akhter, M.P., Enokida, M. & Teshima, R. Effect of parathyroid hormone on cortical bone response to in vivo external loading of the rat tibia. *J Bone Miner Metab* **19**, 244-250 (2001).
31. Robinson, S.T., Shyu, P.T. & Guo, X.E. Mechanical loading and parathyroid hormone effects and synergism in bone vary by site and modeling/remodeling regime. *Bone* **153**, 116171 (2021).

32. Uusi-Rasi, K., *et al.* Effect of alendronate and exercise on bone and physical performance of postmenopausal women: a randomized controlled trial. *Bone* **33**, 132-143 (2003).
33. Kistler-Fischbacher, M., Yong, J.S., Weeks, B.K. & Beck, B.R. A Comparison of Bone-Targeted Exercise With and Without Antiresorptive Bone Medication to Reduce Indices of Fracture Risk in Postmenopausal Women With Low Bone Mass: The MEDEX-OP Randomized Controlled Trial. *J Bone Miner Res* **36**, 1680-1693 (2021).
34. Sims, N.A. & Martin, T.J. Osteoclasts Provide Coupling Signals to Osteoblast Lineage Cells Through Multiple Mechanisms. *Annu Rev Physiol* **82**, 507-529 (2020).
35. Birkhold, A.I., *et al.* Mineralizing surface is the main target of mechanical stimulation independent of age: 3D dynamic in vivo morphometry. *Bone* **66**, 15-25 (2014).
36. Schulte, F.A., Lambers, F.M., Kuhn, G. & Muller, R. In vivo micro-computed tomography allows direct three-dimensional quantification of both bone formation and bone resorption parameters using time-lapsed imaging. *Bone* **48**, 433-442 (2011).
37. Birkhold, A.I., *et al.* Monitoring in vivo (re)modeling: a computational approach using 4D microCT data to quantify bone surface movements. *Bone* **75**, 210-221 (2015).
38. Acevedo, C., Stadelmann, V.A., Pioletti, D.P., Alliston, T. & Ritchie, R.O. Fatigue as the missing link between bone fragility and fracture. *Nat Biomed Eng* **2**, 62-71 (2018).
39. Hernandez, C.J., Lambers, F.M., Widjaja, J., Chapa, C. & Rimnac, C.M. Quantitative relationships between microdamage and cancellous bone strength and stiffness. *Bone* **66**, 205-213 (2014).
40. Lambers, F.M., Bouman, A.R., Rimnac, C.M. & Hernandez, C.J. Microdamage caused by fatigue loading in human cancellous bone: relationship to reductions in bone biomechanical performance. *PLoS One* **8**, e83662 (2013).
41. Mathavan, N., *et al.* Spatial transcriptomics in bone mechanomics: Exploring the mechanoregulation of fracture healing in the era of spatial omics. *Sci Adv* **11**, eadp8496 (2025).
42. Duda, G.N., *et al.* The decisive early phase of bone regeneration. *Nat Rev Rheumatol* **19**, 78-95 (2023).
43. Lambers, F.M., Kuhn, G., Schulte, F.A., Koch, K. & Muller, R. Longitudinal assessment of in vivo bone dynamics in a mouse tail model of postmenopausal osteoporosis. *Calcif Tissue Int* **90**, 108-119 (2012).
44. Webster, D.J., Morley, P.L., van Lenthe, G.H. & Muller, R. A novel in vivo mouse model for mechanically stimulated bone adaptation--a combined experimental and computational validation study. *Comput Methods Biomech Biomed Engin* **11**, 435-441 (2008).
45. Scheuren, A.C., *et al.* Mechano-Regulation of Trabecular Bone Adaptation Is Controlled by the Local in vivo Environment and Logarithmically Dependent on Loading Frequency. *Front Bioeng Biotechnol* **8**, 566346 (2020).
46. Christen, P., van Rietbergen, B., Lambers, F.M., Muller, R. & Ito, K. Bone morphology allows estimation of loading history in a murine model of bone adaptation. *Biomech Model Mechanobiol* **11**, 483-492 (2012).
47. Stadelmann, V.A., Bonnet, N. & Pioletti, D.P. Combined effects of zoledronate and mechanical stimulation on bone adaptation in an axially loaded mouse tibia. *Clin Biomech (Bristol, Avon)* **26**, 101-105 (2011).
48. Alexander, J.M., *et al.* Human parathyroid hormone 1-34 reverses bone loss in ovariectomized mice. *J Bone Miner Res* **16**, 1665-1673 (2001).
49. Bouxsein, M.L., *et al.* Guidelines for Assessment of Bone Microstructure in Rodents Using Micro-Computed Tomography. *Journal of Bone and Mineral Research* **25**, 1468-1486 (2010).
50. Flaig, C. & Arbenz, P. A scalable memory efficient multigrid solver for micro-finite element analyses based on CT images. *Parallel Comput* **37**, 846-854 (2011).
51. Pistoia, W., *et al.* Estimation of distal radius failure load with micro-finite element analysis models based on three-dimensional peripheral quantitative computed tomography images. *Bone* **30**, 842-848 (2002).
52. Nyman, J.S., *et al.* Predicting mouse vertebra strength with micro-computed tomography-derived finite element analysis. *Bonekey Rep* **4**, 664 (2015).
53. Team, R.D.C. R: A language and environment for statistical computing. . in *R Foundation for Statistical Computing* (Vienna, Austria, 2007).